Time dependent processes within the Mexican fields

D5.4

Time dependent processes within the Mexican fields

D5.4

Version 1.0

Jousset Philippe, Tania Toledo, Claudia Finger, Katrin Loehr, Erik Saenger.

Work package 5 – Task 4

2019.11.30

Website: http://www.gemex-h2020.eu

The GEMex project is supported by the European Union's Horizon 2020 programme for Research and Innovation under grant agreement No 727550

Table of Contents[1]

[1] The content of this report reflects only the authors' view. The Innovation and Networks Executive Agency (INEA) is not responsible for any use that may be made of the information it contains.

List of figures

Executive summary

Los Humeros and Acoculco are the two target Mexican geothermal fields of the collaboration study in the GEMex project. These fields represent important examples of superhot and enhanced geothermal systems (EGS) in the Trans-Mexican volcanic belt. Imaging of the deep structures of these study sites is reported in D5.3 in the framework of Task 5.2.

In the present report we summarize the study and the results obtained by innovative approach to detect possible changes in time of the structures found.

During the study period and using only few methods in the time frame of the projects, no clear changes have been detected in the reservoir, which does not exclude there were changes.

1 Introduction

1.1 Objective of the task

In order to understand both the resource amount and the reservoir sustainability, it is mandatory to know as accurately as possible the structure of a geothermal field, the limits of the reservoir, and its change with time. This task is following the work presented in the deliverable 5.2, which was about assessing the structure of the geothermal fields Los Humeros and Acoculco, Mexico, from seismic data acquisition. This report concerns the time dependent processes that modify the structure, due to the exploitation of the reservoirs.

1.2 Limitations of the report

Data was collected during one year and therefore long term possible variations cannot be tracked.

For Acoculco, as there was no activities associated to the geothermal processes and also no earthquakes were recorded during the period of deployment, no attempt to compute or detect time-dependent processes was made, as no changes are expected there. Therefore, we focus only on Los Humeros.

1.3 Structure of the report

There is a link with the deliverable 5.2, as we are focusing here on the change of the structure in the reservoirs.

The report presents 3 different approaches:

1. Study on possible link between fluid injection (data provided by the CFE) induced earthquakes occurence (GFZ, KIT, TNO, OGS)
2. Time-reversal modelling and seismic zone identification (HBO)
3. Beamforming method and time lapse attributes (HBO, GFZ)

The main conclusion is that there was no time dependent processes found during the recording time using the methods used to track them.

2 Time-dependent seismicity and fluid injection

One of the most important drawbacks of reinjection of used fluid after production in geothermal reservoir is the induced seismicity (Zang et al., 2014). The understanding of the induced seismicity is therefore mandatory to understand the impact that the injection can produce on the reservoir. We attempt to derive changes of stress or properties changes in the medium associated to the production at Los Humeros, during the time of deployment of the seismic station of GEMex project (Jousset et al., 2019).

Figure 1 shows the position of the earthquakes recognised within the geothermal field during the seismic array deployment (Jousset et al., 2019). An agglomerative clustering routine (linkage method) was performed to cluster the events in space with a distance threshold of 1km (Chamberlain et al., 2017). These clusters are represented in different colors in Figure 1. Notice the large cluster in the north (green color) close to two injection wells and the cluster in brown close to the third injection well. Those earthquakes are located around the injection wells and were used to produce the seismic tomographic model of the reservoir (Toledo et al., in prep).

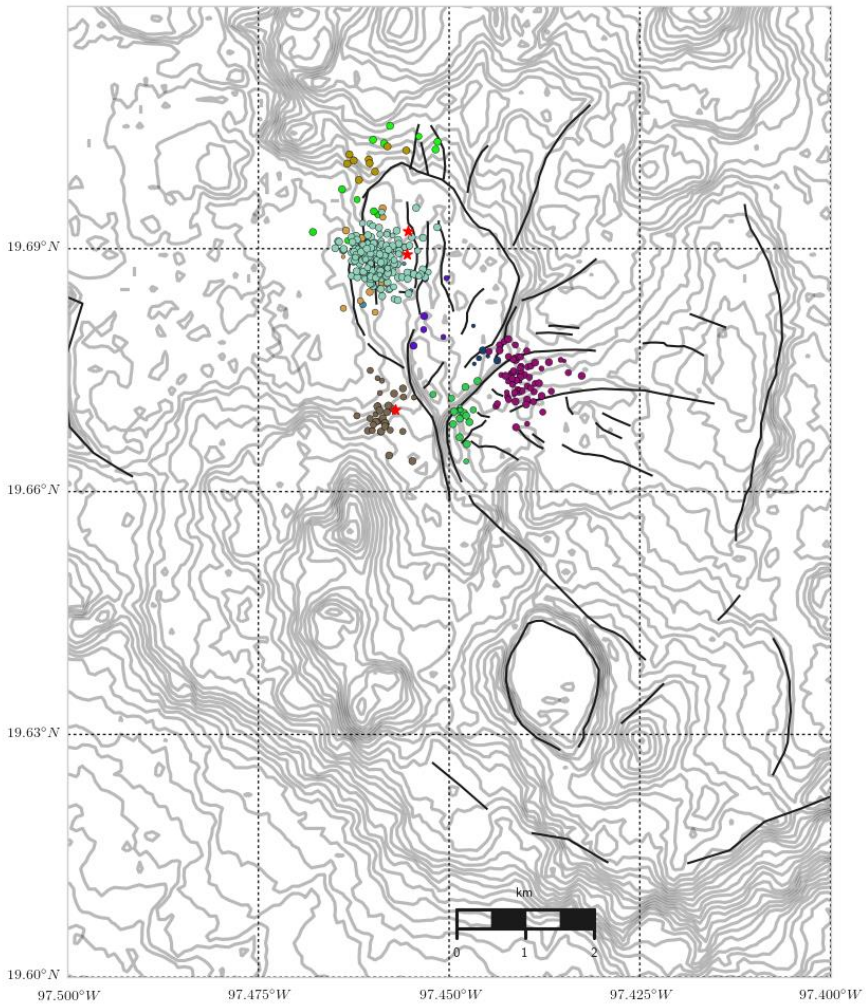

Figure 1 – Topographic map of the Humeros geothermal field with location of the main earthquake clusters detected. Red stars mark the position of injection wells. Note this figure is an update of the map presented in the deliverable 5.2.

During the exploitation of the reservoir, fluid has been reinjected with an average rate of 200 T/h through the 3 wells in Figure 1. The fluid reinjection is probably the cause of the recorded earthquakes, as most of them are surrounding the wells.

Figure 2 shows the insignificant relationship between the daily injection rate and the number of earthquake detected per day during the period of the deployment. The injection rates are kept relatively steady, and so is also the seismicity rate.

We conclude that the reinjection of fluid in Los Humeros, during the time of the experiment (2018) did not produce noticeable changes in the reservoir.

Overall the earthquakes in these clusters are also included in the tomographic model of the reservoir (Toledo et al., in prep). The results described in this document are associated to the (Toledo et al., 2019) seismic dataset.

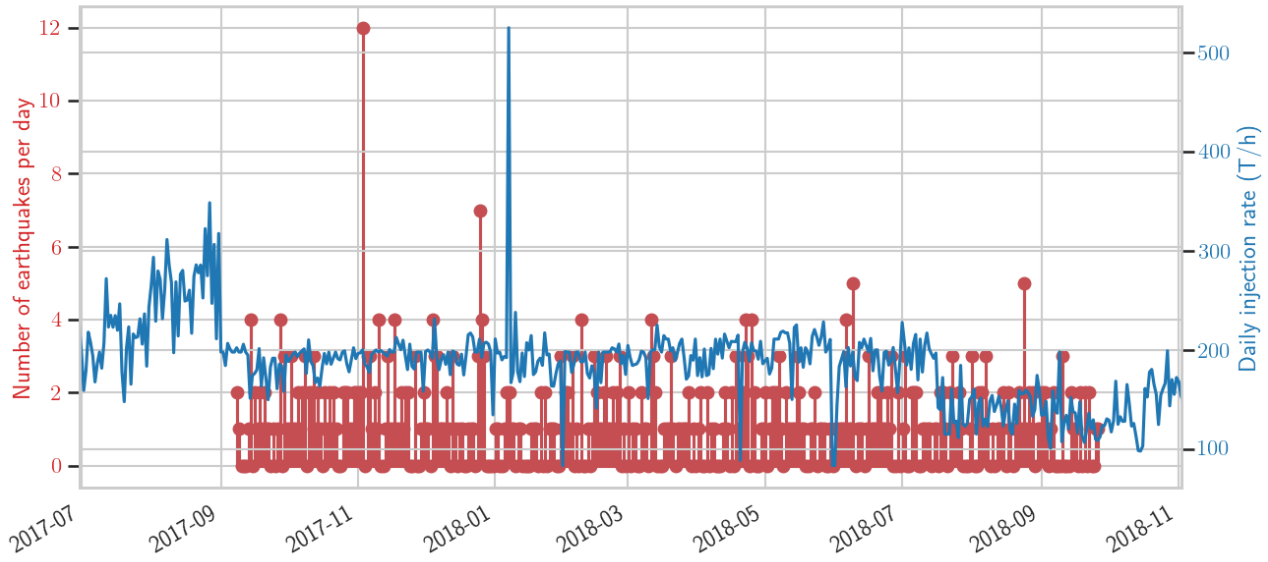

Figure 2 – Daily injection rate and number of earthquakes detected per day considering only the two main clusters surrounding the wells during the whole period of deployment of the seismic network. It appears that the daily rate of earthquake does not change significantly.

3 Time-reverse imaging in Los Humeros

Introduction

Time-reverse imaging (TRI) is a method for locating and characterising seismic events. In contrast to other localisation methods, TRI does not rely on the identification of events and their onset times in seismic traces. Therefore, TRI is exceptionally well-suited for locating events with a low signal-to-noise ratio or events that occur quasi-simultaneously.

For TRI, seismic traces are reversed in time and inserted into an adequate velocity model at the positions corresponding to their recording points. The time-reversed wavefield is then back propagated through the model using, in this case, a finite-difference scheme based on the rotated staggered grid approach (Sanger, 2000). The wavefield ideally focuses on the location where the event occurred at the time the event occurred. Additionally, an illumination map is produced using a noise wavefield as proposed by Witten (2011) to eliminate areas of high energy caused by the sparse stations at the surface and specific velocity structures such as low-velocity zones. To analyse the focusing of the wavefield, four imaging conditions may be used (Saenger, 2011): the total energy density, the P-wave energy density, the S-wave energy density and the maximum displacement.

Results

In the scope of this project, TRI is applied to locate micro-seismic sources at the geothermal reservoirs Los Humeros and Acoculco in Mexico. However, before the real-life events can be located, synthetic studies are performed to investigate the behaviour of TRI on the reservoir scale and estimate the obtainable location accuracy. An extensive numerical study is published as Werner (2018) and describes location accuracy in relation to the station distribution, a complex velocity structure and low signal-to-noise ratios. An extreme sensitivity of the source location accuracy to the station distribution was observed which led to the discovery of rules for optimal station networks to be used with TRI.

A recently submitted manuscript (Finger and Saenger, 2019), proposes a work flow for the estimation of the source-location accuracy when a station network and velocity model is given. This study underlines that the station distribution has a higher influence on the location accuracy than the velocity structure itself. However, the velocity model was assumed to be perfectly known in this study. The spatial variation of the source-location accuracy, coined sensitivity maps, appears very complex. These sensitivity maps may significantly increase the source-location accuracy of real-life events by providing areas where even under best circumstances no localization is possible. These areas may be excluded when locating events and thus artificial localizations are drastically reduced.

Sensitivity Maps for Los Humeros were created using the location of the 27 stations of the dense network. The seismic station network is described in detail in Deliverable 5.3 (Jousset et al., 2019). Furthermore, the most sophisticated velocity model at this time is the one-dimensional velocity model from Löer et al. (2019). An adapted velocity model based on Löer et al. (2019) was used in this study to estimate location accuracies. 36 sources were placed in a grid with an inter-source distance 2.4 km and in eleven depths each. Sensitivity maps are created once for strike-slip sources (only $M_{xy} \neq 0$) and once for explosion sources ($M_{xx} = M_{yy} = M_{zz} \neq 0$). As a source signal for all sources, a Ricker wavelet with a central frequency of 5 Hz was used. The model size was chosen to be 20 km x 20 km with a depth of 15 km and the grid spacing was set to 20 m. The origin of the model was set in the centre at the surface, which corresponds to 19° 40.2’ N and 97° 27’ E.

The sources are excited simultaneously and located using the described TRI method and from the images obtained by the imaging conditions, the spatial and temporal error is calculated as the distance of each source to the nearest localisation. Sources are separated into three categories: 1) High accuracy localisation with a spatial error smaller than half the S-wave wavelength and a temporal error smaller than half a period and a spatial error that is smaller than the focus radius. 2) Medium accuracy localisations that are less accurate than the high accuracy localisations. 3) Insufficient accuracy are sources that could not be located.

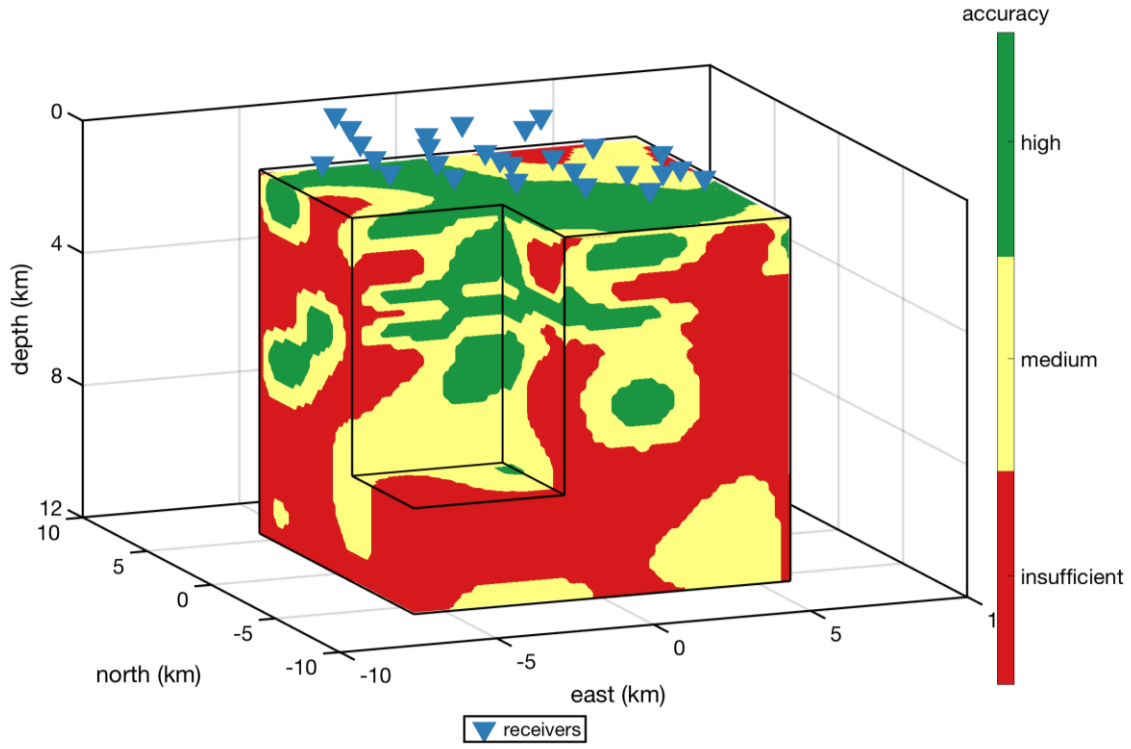

Figure 3: Sensitivity map for 36 explosion sources in 11 depths each. Only the area where sources were placed is colored. 27 stations deployed in Los Humeros are used and a velocity model based on Löer et al. (2019) is used.

In Figure 3, the sensitivity map is shown for the explosion sources. Sources can be located to a depth of about 6 km and generally below the surface stations. However, in general, the spatial variation of accuracies presents quite complex.

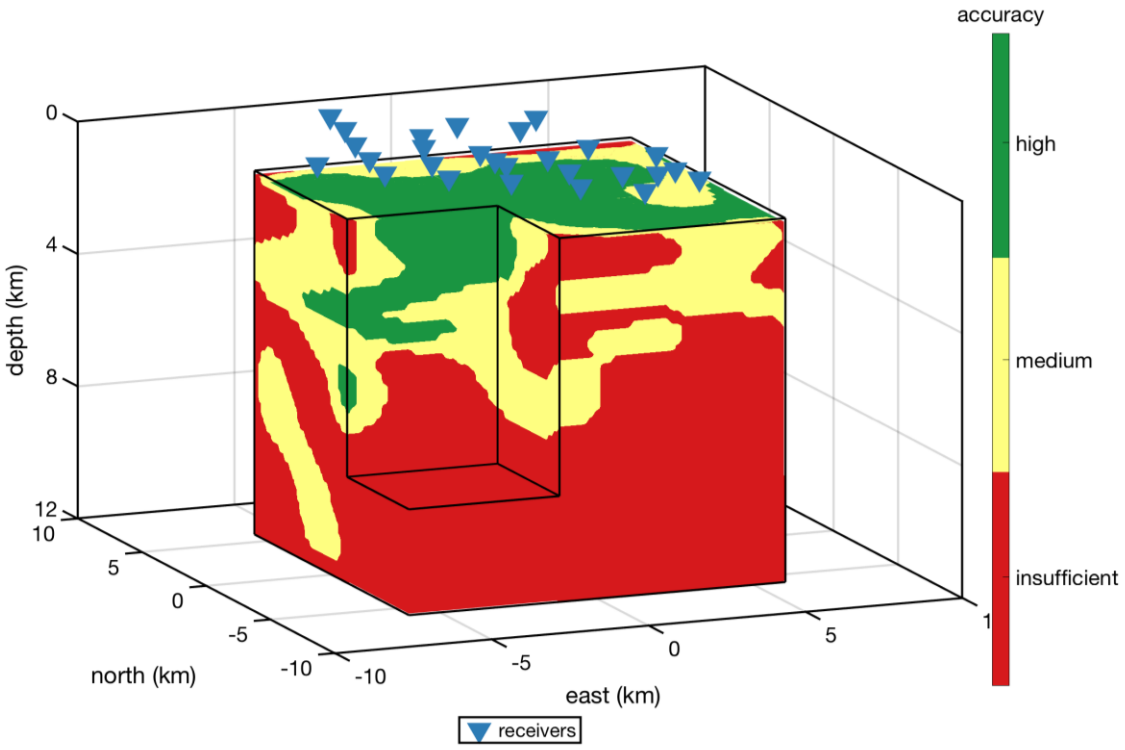

Figure 4: Sensitivity map for 36 strike-slip sources in 11 depths each. Only the area where sources were placed is colored. 27 stations deployed in Los Humeros are used and a velocity model based on Löer et al. (2019) is used.

In Figure 4, the sensitivity map is shown for the strike-slip sources. The distribution of accuracies appears to be different than for explosion sources. Sources can only be located to a depth of about 5 km. If a detailed interpretation is done in context with, for example, well locations, multiple source types should be considered. However, since seismic events are rarely of one pure source types, the number of sensitivity maps could be endless when considering all source types. Therefore, we propose to use sensitivity maps with explosion sources and keep in mind that other source types may be located in parts where explosion sources cannot and vice versa.

Outlook

The sensitivity maps for the geothermal field of Los Humeros highlight the complexity of the spatial variation in the source-location accuracy and the necessity to assess the accuracy for each project individually. In general, the influence of the station geometry on the source-location accuracy is larger than the influence of the velocity model. This means that the most significant increase in accuracy for TRI may be achieved by optimizing the station network. The sensitivity maps presented here will be used to locate micro-seismic events in Los Humeros in the future and are believed to significantly enhance the location accuracy of these real-life events.

4 Beamforming method

4.1 1D velocity profiles from three-component beamforming

Three-component (3C) beamforming is an array technique that provides estimates of the dominant polarization (wave type), direction of arrival (azimuth), velocity, and incidence angle of a seismic wave field (here, ambient noise) crossing the array in a given time-frequency window. We have shown in Deliverable 5.3 how this analysis is based on wavenumber measurements and how the resolvable wavenumber range depends on the size and geometry of the seismic array. By taking wavenumber measurements at different frequencies, the dispersive character, that is, the frequency dependence of surface wave velocities can be observed. Since different frequencies are sensitive to different depths, the dispersion analysis, when put into an inversion scheme, provides a 1-dimensional velocity profile of the subsurface below the array. We use the reversible-jump Markov chain Monte Carlo inversion method (called rj-McMC) to extract a shear-velocity profile from Rayleigh wave dispersion curves retrieved from ambient noise beamforming.

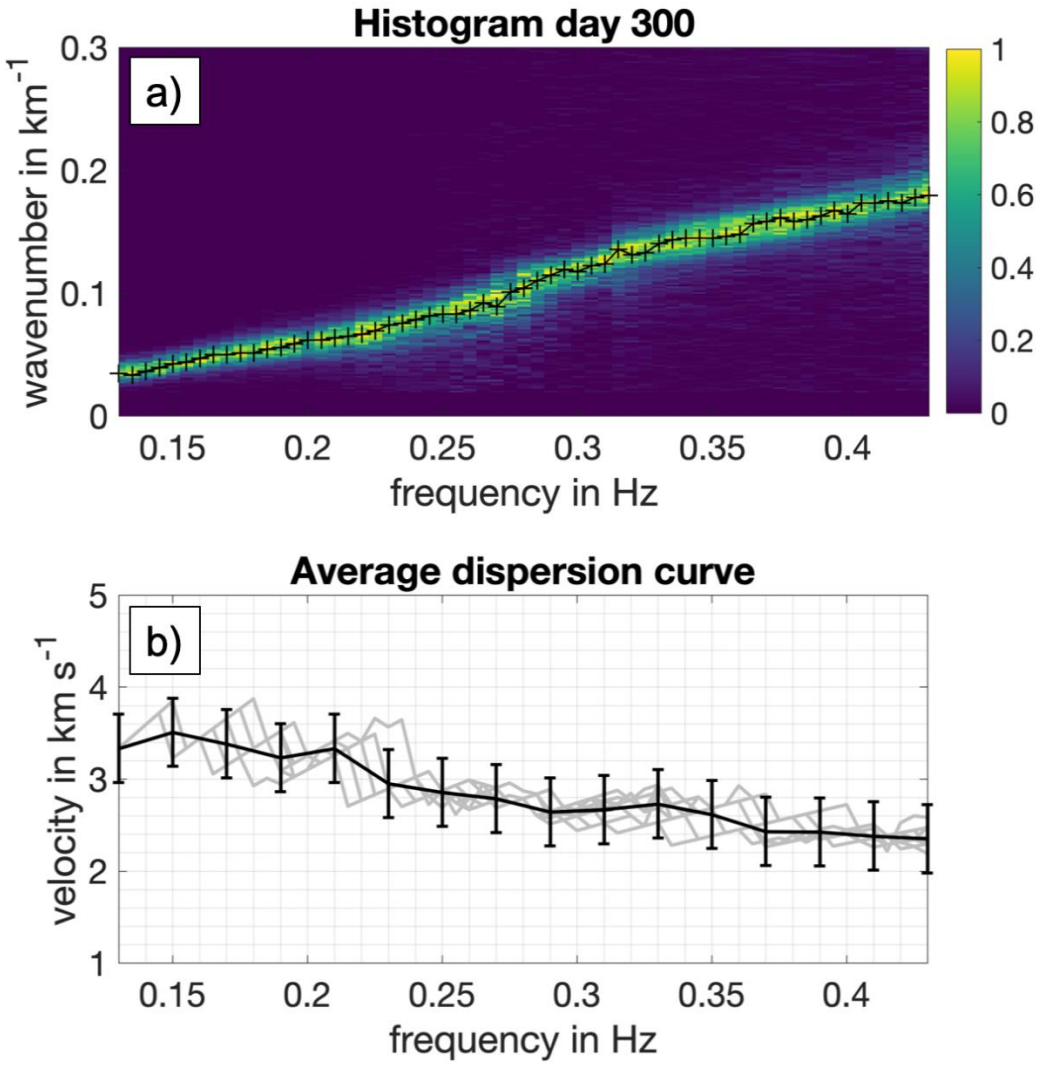

Figure 5 - (a) Two-dimensional histogram showing wavenumber versus frequency of retrograde Rayleigh wave detections on day 300 (2017), normalised per frequency. Black crosses mark wavenumber bins with maximum number of detections per frequency, $k(f)$. (b) Average dispersion curve (black) providing phase velocity as a function of frequency, $c(f)$, computed from 10 daily dispersion curves (grey) and down sampled to $\Delta f = 0.2\ Hz$. Black error bars indicate twice the average standard deviation. Daily dispersion curves were derived from histogram maxima as shown in (a) using $c(f) = f/k(f)$.

Figure 5a provides an example for such a dispersion curve taken from a two-dimensional histogram showing wavenumber versus frequency of retrograde Rayleigh waves detected on a single day. In Figure 5b, an average dispersion curve has been computed from 10 daily dispersion curves, which serves as input to the inversion scheme. The rj-McMC method is a Bayesian inversion scheme that updates a prior probability distribution that describes information about model parameters (velocities with depth) that is independent of the current data, with information added by the data (i.e., the dispersion curve). This results in a posterior distribution of parameters. The rj-McMC algorithm allows the dimensionality of the parameter space, that is, the number, depth-extent, and seismic velocities of horizontal layers of the medium, to vary in the inversion. Each run of rj-McMC generates a chain of 2 Mio samples (example velocity models) which are distributed according to the posterior distribution as the number tends to infinity. To obtain approximately independent samples, we retain only every 250th sample after the first 0.5 Mio samples in each of 12 independent chains for analysis. The density of the final set of retained samples represents the posterior probability density function (PDF) of shear velocity with depth.

4.2 Shear-velocity profile of the Los Humeros caldera

The PDF obtained for the Los Humeros area is shown in Figure 6a. Zero level corresponds to 2.9 km above sea level, which is the average topographic height of the seismic stations considered. The colour scale has been normalised with respect to the maximum number of samples at each depth level. Yellow colours indicate velocities of higher probability compared to blue colours. The solid white curve denotes the maximum likelihood of the PDF. For comparison, the dotted white curve shows the shear velocity profile retrieved from earthquake analysis by Toledo et al. (pers. comm.). In Figure 6b, we display a shear velocity profile that combines the results from both methods: down to 4.0 km, this combined profile is based on earthquake data (dotted white curve in Figure 6a), below 4.0 km, it follows ambient noise beamforming results (solid white curve in Figure 6a). Background colours in Figure 6b indicate different geological sections as described in the legend. Section transitions are based on prominent discontinuities in the shear-velocity profile (around 0.9 km, 1.8 km, 5.1 km, and 10.5 km depth) and roughly correspond to average transition depths observed in well logs, that is, for those transitions that were actually sampled. The rocks of the Teziutlan massif have been observed in outcrops north of the Los Humeros geothermal site, however, at the locations of the wells they are too deep to be observed in-situ. The shear-velocity profile implies that the transition from the sedimentary basement to the Teziutlan massif occurs in about 5.1 km depth, where shear velocities increase abruptly from around 2.6 km s^{-1} to 3.3 km s^{-1}. The decline in shear velocity observed at about 10.5 km depth is interpreted as the onset of the brittle-ductile transition, which typically correlates with a decrease in shear strength (e.g., Imber et al., 2008). Constraining the extent of rocks with brittle behaviour and permeability conditions at depth, these results are of paramount importance for the future exploitation of the deeper reservoir and provide a basis for the geological and thermodynamic modelling of active superhot geothermal systems in general.

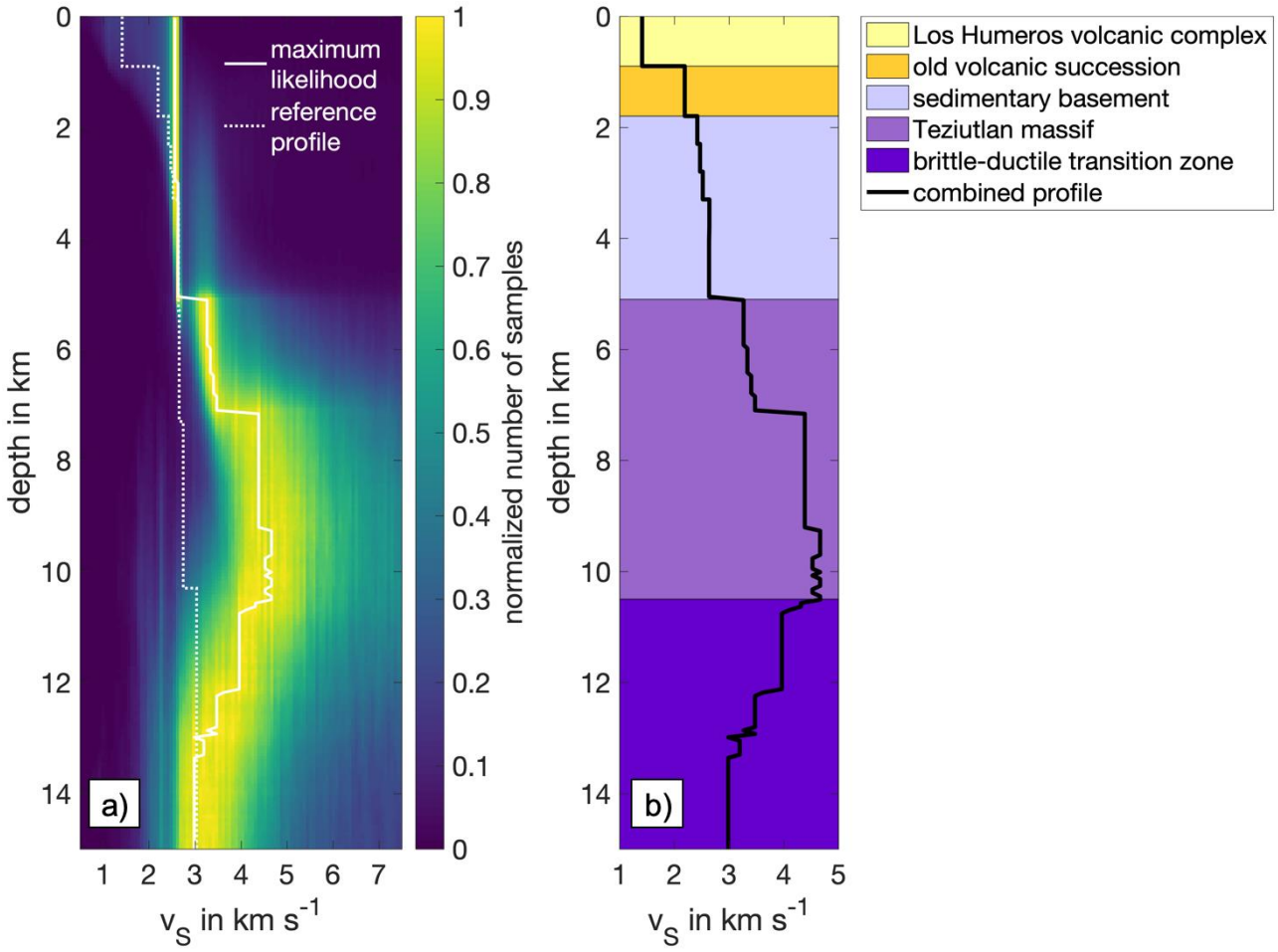

Figure 6 - (a) Probability density function (PDF) of shear-velocity distribution as retrieved from rj-McMC inversion, normalised per depth level. The white, solid curve indicates maximum likelihood of the PDF, the white, dotted curve represents the profile retrieved from the analysis of earthquake data and is plotted for comparison. (b) Combined shear-velocity profile (black) from the analysis of earthquake data (dotted curve in (a), down to 4 km depth) and ambient noise beamforming (solid curve in (a), below 4 km); background colours indicate geological structure (see legend).

4.3 Temporal monitoring

Since ambient noise is continuously available, the beamforming analysis can be repeated for different time periods during the recording time of the seismic array, given that a sufficient amount of stations is available. For each time period a new velocity profile can be derived, and thus potential temporal variations of the subsurface structure can be monitored. It is important, however, to account for changes in the station geometry and the noise source distribution to not mistake them for structural changes. Hence, in theory, subsurface monitoring with ambient noise beamforming presents a low-cost and easy-to-implement addition to expensive active seismic experiments.

At the Los Humeros array, however, the number of available stations changed a lot during the recording time due to malfunctioning of individual stations or vandalism. Thus, for many time periods not enough stations where available to obtain reliable beamforming results.

5 Conclusion

5.1 Scientific knowledge increased

It seems to the first sight that the injection in Los Humeros did not produce any temporal changes in the reservoir.

This result has at least two significations:

1. We could not detect any changes in the reservoir during the experiment
2. The level of injection seems optimal for not changing the reservoir production ability.

6 References

Chamberlain, C. J., Hopp, C. J., Boese, C. M., Warren-Smith, E., Chambers, D., Chu, S. X., Michailos, K., Townend, J., EQcorrscan: Repeating and near-repeating earthquake detection and analysis in Python. Seismological Research Letters, 2017.

Finger, C. and Saenger, E. H.: Sensitivity Maps for Time-Reverse Imaging: An Accuracy Study for the Los Humeros Geothermal Field (Mexico), GJI, 2019. *Submitted*

Jousset P., K. Agustsson, E. Barison, G. Böhm, M. Caló, I. G. Chavarria, B. Farina, E. Gaucher, K. Loer, J. Martins, M. Perton, F. Poletto, E. Saenger, A. F. Soto, T. Toledo, A. Verdel, C. Werner. Seismic structures of the Acoculco and Los Humeros geothermal fields. Work package 5 – Task 2, 2019.04.30, Deliverable report.

Löer K., Toledo T., Norini G., Zhang, X., Curtis A. and Saenger E.H.: Imaging the deep structures of the Los Humeros geothermal field, Mexico, using three-component ambient noise beamforming, 2019. *in preparation*

Saenger, E. H., Gold, N., and Shapiro, S. A.: Modeling the propagation of elastic waves using a modified finite-difference grid, Wave Motion, 31, 77–92, https://doi.org/10.1016/S0165-2125(99)00023-2, 2000.

Saenger, E. H.: Time reverse characterization of sources in heterogeneous media, NDT E. Int., 44, 751–759, https://doi.org/10.1016/j.ndteint.2011.07.011, 2011.

Toledo, Tania; Gaucher, Emmanuel; Metz, Malte; Calò, Marco; Figueroa, Angel; Angulo, Joel; Jousset, Philippe; Kieling, Katrin; Saenger, Erik (2019): Dataset of the 6G seismic network at Los Humeros, 2017-2018. GFZ Data Services. Other/Seismic Network. doi:10.14470/1T7562235078.

Witten, B. and Artman, B.: Signal-to-noise estimates of time-reverse images, Geophysics, 76, MA1–MA10, https://doi.org/10.1190/1.3543570, 2011.

Werner, C. and Saenger, E.H.: Obtaining reliable source locations with time reverse imaging: limits to array design, velocity models and signal-to-noise ratios, Solid Earth, 9, 1487-1505, https://doi.org/10.5194/se-9-1487-2018, 2018.

Zang A. Oye V., Jousset P., Deichmann N., Gritto R., McGarr A and Bruhn D. Analysis of induced seismicity in geothermal reservoirs – an overview. Geothermics 52, 6-21. https://doi.org/10.1016/j.geothermics.2014.06.005.

7 Acknowledgements

The authors thank the Comisión Federal de Electricidad (CFE, Mexico) for providing their data for this research and access to the geothermal sites in Los Humeros and Acoculco. We are especially thankful for the opportunity to deploy the passive seismic station network at Los Humeros.

The authors thank Marco Calò (UNAM), Angel Figueroa Soto (UMSNH) and Joel Angulo (UNAM) for their collaboration and the enormous work during the execution of the passive seismic experiment.

Coordination Office, GEMex project

Helmholtz-Zentrum Potsdam
Deutsches GeoForschungsZentrum

Telegrafenberg, 14473 Potsdam

Germany